Applied Catalysis B: Environment and Energy 344 (2024) 123638

Contents lists available at ScienceDirect

Applied Catalysis B: Environment and Energy

journal homepage: www.elsevier.com/locate/apcatb

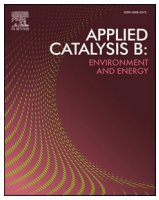

Electrocatalytic ethanol-to-CO_2 selectivity on the Ir electrode: A quasi-quantitative electrochemical infrared absorption spectroscopic investigation

Rui-Lin Wei [1], Yue Liu [1], Yao-Yue Yang [*,2]

Key Laboratory of General Chemistry of the National Ethnic Affairs Commission, School of Chemistry and Environment, Southwest Minzu University, Chengdu 610041, Sichuan, China

ARTICLE INFO

Keywords:
Iridium
C1 pathway
ATR-SEIRAS
IRAS
TIAS
HPLC

ABSTRACT

Ir has long been regarded as an alternative ethanol-to-CO_2 electrocatalyst, but little is known about the ethanol oxidation reaction (EOR) mechanism on Ir, especially the C1 pathway selectivity. Thereby, in situ quasi-quantitative electrochemical infrared absorption spectroscopy (QEIAS), consisting of total-reflection surface-enhanced infrared absorption spectroscopy (ATR-SEIRAS), infrared absorption spectroscopy (IRAS), and transmission infrared absorption spectroscopy (TIAS) with a thin-layer flow cell, is established to probe it. Initially, the well-accepted EOR dual-pathway mechanism is confirmed via ATR-SEIRAS and IRAS. Ir-H_{ad} species (ca. 2040 cm^{-1}), originating from the ethanol dissociation at low potentials, are observed for the first time to replenish the reaction process. Based on it, the apparent Faradaic efficiency of the C1 pathway (FE_{C1}) is readily estimated to be as high as 76.4% (0.7 V) in acidic media. The quantitative analysis of reaction residual verifies these FE_{C1} results through high-performance liquid chromatography (HPLC), and a relative error of only 2–9% exists between the two methods. Thus, Ir might be more efficient for ethanol complete oxidation than other Pt-group metallic catalysts, especially in acidic media. This work could be necessary for the rational design of Ir-based EOR catalysts with high C1 pathway selectivity and low over-potential for direct ethanol fuel cells.

1. Introduction

Net-zero carbon emissions have been one of the hottest topics all around the world right now, which is vital to limit global warming to 1.5 °C and thus avoid the word worse climate change. To reach net zero around mid-century, the energy policy, technology, and behavior need to shift across the board. As for the energy supply technology, the share of renewable and sustainable energy should be increased in the energy mix, which could be projected to supply 70–85% of electricity by 2050 [1,2]. Among various new energy devices, Direct Alkaline Ethanol Fuel Cells (DAEFCs) are considered as the promising portable low-carbon power devices due to the high mass density, safety, and environment-friendly [3–6]. The use of alkaline media not only benefit the utilization of low-Pt and/or Pt-free catalysts [7], but also reduce the CO_2 emission through the neutralization reaction between CO_2 and the alkaline solution. Nevertheless, the sluggish kinetics and low selectivity of the complete ethanol oxidation reaction (EOR) impeded the energy conversion efficiency of DAEFCs [8]. Generally, EOR follows a so-called dual-pathway mechanism (i.e., C1- and C2-pathway), and the C-C bond cleavage is critical to improve the C1-pathway faraday efficiency [9,10]. So, it is urgent to explore highly active catalysts to break the C-C bond to let EOR follow the 12-electron reaction pathway.

Pt-group metallic catalysts have been the most effective electrocatalysts for EOR so far [11–14]. In detail, Pt-based catalysts are active for EOR both in acidic and alkaline media, whereas Pd-based catalysts only work in alkaline media [4,9]. Recently, some EOR catalysts have been developed to obtain the high C1 faraday efficiency. However, they still suffer CO poisoning and thus low activity and C1-pathway selectivity at low oxidation potential, which is difficult to meet the requirements of application of fuel cells [15–18]. In this context, García et al [19]. reported a PtAuSn/W_2C catalyst to obtain a lower EOR onset potential and higher C1 pathway selectivity due to the

* Corresponding author.
E-mail address: yaoyueyoung@swun.edu.cn (Y.-Y. Yang).
[1] These authors contributed equally.
[2] ORCID ID: 0000–0002-4573–9437

https://doi.org/10.1016/j.apcatb.2023.123638
Received 25 July 2023; Received in revised form 16 November 2023; Accepted 15 December 2023
Available online 19 December 2023

supported effect in acidic media. Gallant et al [20]. prepared the hollow structured Pt−Rh electrocatalysts to achieve a higher C1-pathway faradaic efficiency(FE) of 38.3% and longer durability derived from confinement effects in alkaline media.

On the other hand, Rh and Ir were found to be the effective catalytic component for splitting the C-C bond of ethanol [21–25], which provided a possibility for improving the faraday efficiency of ethanol complete oxidation at low potential. After that, Rh-based EOR catalysts were consecutively reported in alkaline media, such as Rh/CeO_2 [26], cyclic Penta-twinned Rh nanobranches [27], and excavated RhNi nanobranches [28]. Meanwhile, Teng et al. demonstrated that ethanol could be effectively broken at the Rh surface through gas chromatography–mass spectrometry (GC-MS) and online membrane inlet mass spectrometer (MIMS) study [29]. We also investigated the EOR on the Rh surface at the molecular level, which found the potential-dependent C1 pathway selectivity of EOR at Rh in alkaline media. And we also proposed that the oxyphilic components around Rh sites that can provide the oxygenated species (i.e., OH_{ad}) should be the key to obtaining a high-efficiency EOR catalyst [7]. Along this line, Rh-PbO_x [30], Rh-Bi $(OH)_3$ catalysts [31] were respectively designed and fabricated in our previous work, which improved the C1 faraday efficiency to 25–30% in alkaline media, as well as the mass activity by ca. 3500 mA mg_{Rh}^{-1}. Therefore, it can be claimed the mechanistic study of EOR could be important for the designing and preparation of effective EOR catalysts.

Similarly, Ir was also believed to effectively enhance the activity of EOR and improve the C1 pathway selectivity both in acidic and alkaline media, which is much different from what is found at the Rh and Pd surfaces [32–35]. Note that, Ir was previously used as the co-catalytic component to cut the C-C bond, such as the reported catalysts of PdCoIr tetrahedron [36], $PtIrSnO_2$ [21], PtIr core-shell nanocubes [33] and Au@PtIr core-shell catalysts [32]. Meanwhile, Ir-based catalysts such as Ir-Sn/C, Ir-Ru/C [37,38], Ir_3Pb nanodendrites [34] and Ir-Bi_2O_3 [39] were also prepared and showed better EOR activity, CO_2 selectivity than commercial Pt/C. Nevertheless, Ir-based catalysts show lower activity and C1 pathway selectivity than that the catalysts using Ir as the auxiliary catalytic component. Referring to our development process of Rh-based EOR catalysts [30,31,40], it's essential to study EOR at Ir at the molecular level to rationally direct the catalysts' design and preparation. Nevertheless, as far as we know, the relative mechanistic investigation on EOR at the Ir surface can be hardly found, especially the understanding of reaction intermediates and product distribution during the EOR at the Ir surface.

Regarding the investigation of interfacial electrochemical processes, in-situ electrochemical attenuated total-reflection surface-enhanced infrared absorption spectroscopy (ATR-SEIRAS) can effectively and directly provide molecular-level information of surface adsorbed species due to its high surface-sensitivity and simple surface selection rule [9,41–43]. On the other hand, in-situ electrochemical infrared reflection absorption spectroscopy (IRAS) can readily detect the dissolved products confined in the thin-layer between the electrode and infrared window [44,45]. In-situ FTIR also was used to measure the CO_2 selectivity for EOR via the peak integration method developed by Weaver et al. in acidic media [46]. Correspondingly, in alkaline media, we developed a method to quasi-quantitative analysis of the products with the help of the thin-layer transmitting infrared absorption spectroscopy (TIAS) under a continuous flowing mode [7,40]. Thus, an in situ quasi-Quantitative Electrochemical Infrared Absorption Spectroscopic (QEIAS) method can be readily established by combining in situ electrochemical ATR-SEIRAS, IRAS, and TIAS based on the Beer-Lambert Law. It can effectively provide a potential-dependent variation of surface-adsorbed intermediates and the dissolved products, which ensures the possibility of clarification of the electrocatalytic reaction mechanism from a quasi-quantitative view. To obtain the FE_{C1} potential dependent during EOR on Ir more accurately, the ^1H nuclear magnetic resonance (^1H NMR) and the high-performance liquid chromatography (HPLC) are used to analyze the C2 products in the residual electrolyte.

Thereby, in this work, we studied the process of ethanol adsorption, self-dissociation, and oxidation on Ir electrodes by in situ QEIAS, ex-situ ^1H NMR and HPLC both in acidic and alkaline media. The results may replenish the EOR dual-pathway mechanism and be meaningful in directing the development of high-performance EOR Ir-based catalysts.

2. Experimental

2.1. in situ electrochemical ATR-SEIRAS

Typically, a ca. 60 nm thick SEIRA-active Au film was electroless deposited on the Si ATR prism surface via the previously reported routine [47]. Then, the Si prism was fixed onto a homemade spectro-electrochemical cell to form the three-electrode system, using Au film as the working electrode (WE), an ultrapure graphite rod, and a saturated calomel electrode (SCE) as the counter electrode (CE) and reference electrode (RE), respectively. Then Ir nanofilm can be electrochemically deposited on the Au under-layer by the cyclic voltammetry (CV) scanning (ca. 120 cycles) between − 0.25 V to 0.4 V (vs. SCE) in 5 mM H_2IrCl_6 + 0.5 M H_2SO_4 plating solution at ca. 333 K [42,48,49].

Thus in situ Electrochemical ATR-SEIRA spectral measurements on the Ir film electrode can be carried out in a homemade ATR-mode optical system (Fig. S1A). It should be guaranteed that IR radiation could penetrate the Si prism into the interfacial boundary of the Si/Au/Ir film layer at an incident angle of ca. 70°. The real-time ATR-SEIRA spectra were simultaneously collected while ethanol was dosing to Ir film electrode surface or ethanol electro-oxidation reaction on the Ir electrode was ongoing, with a time resolution of 5 s for each spectrum.

2.2. in situ electrochemical IRAS and thin-layer TIAS

The IRAS configuration was the same as what was described previously (Fig. S1B) [7,16,50]. Specifically, the Ir working electrode could be obtained by electro-deposition on a Φ= 5 mm smooth Au disk electrode as the above-mentioned method. Before spectra collecting, a thin-layer solution (~10 μm) should be obtained by pressing the Ir disk electrode onto the CaF_2 IR window, and the IR beam sequentially passed through the CaF_2 window, the thin-layer solution and then reflected by the Ir electrode surface at an incident angle of ca. 55°. The sample and reference spectra can be acquired at corresponding electrode potentials. The electrode could be lifted fully and carried out electrochemical cleaning at the potential region of hydrogen adsorption and desorption before recording each spectrum [16]. Every spectrum was generated by average co-adding 256 interferograms to reach a better signal-to-noise (S/N) ratio.

The thin-layer transmission IR spectra (TIAS) of 0.02–0.05 M CH3COONa and 0.05 M CH3COONa + 0.005 ~ 0.02 M Na_2CO_3 were obtained through an infrared spectroscopic flow-cell (PIKE-162–1100) [7]. This flow cell consists of two CaF2 disks and one of them is drilled into two small holes as the inlet and outlet of liquid samples, respectively. A 25-μm-thick Teflon gasket was placed between two CaF2 disks to form a thin layer. Thus, the sample solution and pure water could be readily injected into this thin layer through the inlet hole to collect the sample and reference spectrum (co-adding 256 interferograms).

The infrared spectra were collected by an Agilent Cary 660 FTIR with the liquid-nitrogen-cooled mercury-cadmium-telluride (MCT) detector. The collected spectra are presented as a unit of absorbance (Abs.) versus wavelength (cm^{-1}), and all spectral resolution is 8 cm^{-1}. The unit of absorbance is defined as $-\log(I/I_0)$, where I and I_0 are the infrared light intensity at sample and reference conditions, respectively. Thus, the upward bands represent the generated species during the spectra collection, while the downward bands in this work mean the consumed species.

2.3. ^1H NMR and HPLC

To confirm the EOR product distribution, the residual solution was pulled out to be qualitatively measured by ^{1}H NMR that was acquired on a Bruker AVANCE NEO 400 spectrometer. The ^{1}H NMR samples were prepared by mixing 500 μL residual solution + 100 μL D_2O + 10 μL dimethyl sulfoxide (DMSO) in the NMR tubes. On the other hand, the quantitative analysis of the C2 products concentration in the residual solution can be realized by HPLC measurements with the help of the external standard method, and thus C1 pathway Faradaic efficiency (FE_{C1}) of EOR can be calculated using the following equations:

$$Q_{C2} = \frac{C_{C2} \times V \times z \times F}{M} \quad (1)$$

$$FE_{C1} = 1 - \frac{\sum Q_{C2}}{Q_{total}} \quad (2)$$

Where C_{C2} is the concentration of the certain C2 product obtained from HPLC, F is the Faraday constant equal to 96,485 C mol^{-1}, z is the number of electron transfer for the corresponding product, V is the volume of the electrolyte, and M is the molar mass of the product. Q_{C2} is the charge for producing a certain C2 product, and Q_{total} is the total Coulombs during the whole EOR process. To estimate the C_{C2}, the residual solution was diluted in a 50 mM H_2SO_4 solution by appropriate multiple, and then injected into a HPLC (FULI, LC-5090) with an ultraviolet-visible (UV-Vis) detector (UV-210 nm). A sugar column (ChromCore Sugar-10 H, 6 μm, 7.8 × 300 mm) was used to proceed with separation of solution components at a column temperature of 35 ℃. As well, a 25 mM H_2SO_4 aqueous solution was made as the eluent with its flowing rate of 1 mL min^{-1}. Before the quantitative calculation of the C2 products, the corresponding external standard curves in a suitable concentration range should be established with standard samples in advance.

A CHI-660 electrochemistry workstation was used to control the applied potentials and record the current. All potentials in this work quoted with the SCE were further transferred to the reversible hydrogen electrode (RHE) via a simple Nernst equation unless noted otherwise. All chemicals used here are guaranteed reagents (GR), and all solutions were freshly prepared with ultrapure Mill-Q water (18.25 MΩ·cm) before each measurement. All measurements were made at room temperature 25 ± 2 °C.

3. Results and discussion

3.1. EOR dual-pathway mechanism

3.1.1. Ethanol self-dissociation

Ethanol self-dissociation on catalysts' surface under open circuit potential (OCP) is an important prepositional surface process (if any) [9]. In Fig. 1 A and C, with injecting ethanol onto the Ir film electrode in 0.1 M $HClO_4$, the OCP decreased from ca. 0.86 V to 0.2 V rapidly and then stabilized at ca. 0.35 V within 100 s; Similarly, it also dropped from ca. 0.89 to 0.2 V and then stabilized at 0.25 V in 0.1 M NaOH. The OCP at Ir/ethanol interface locates at the hydrogen adsorption/desorption potential region, especially in alkaline media (see Fig. 4 below), which indicated H_{ad} species could adsorb on the Ir surface after introducing

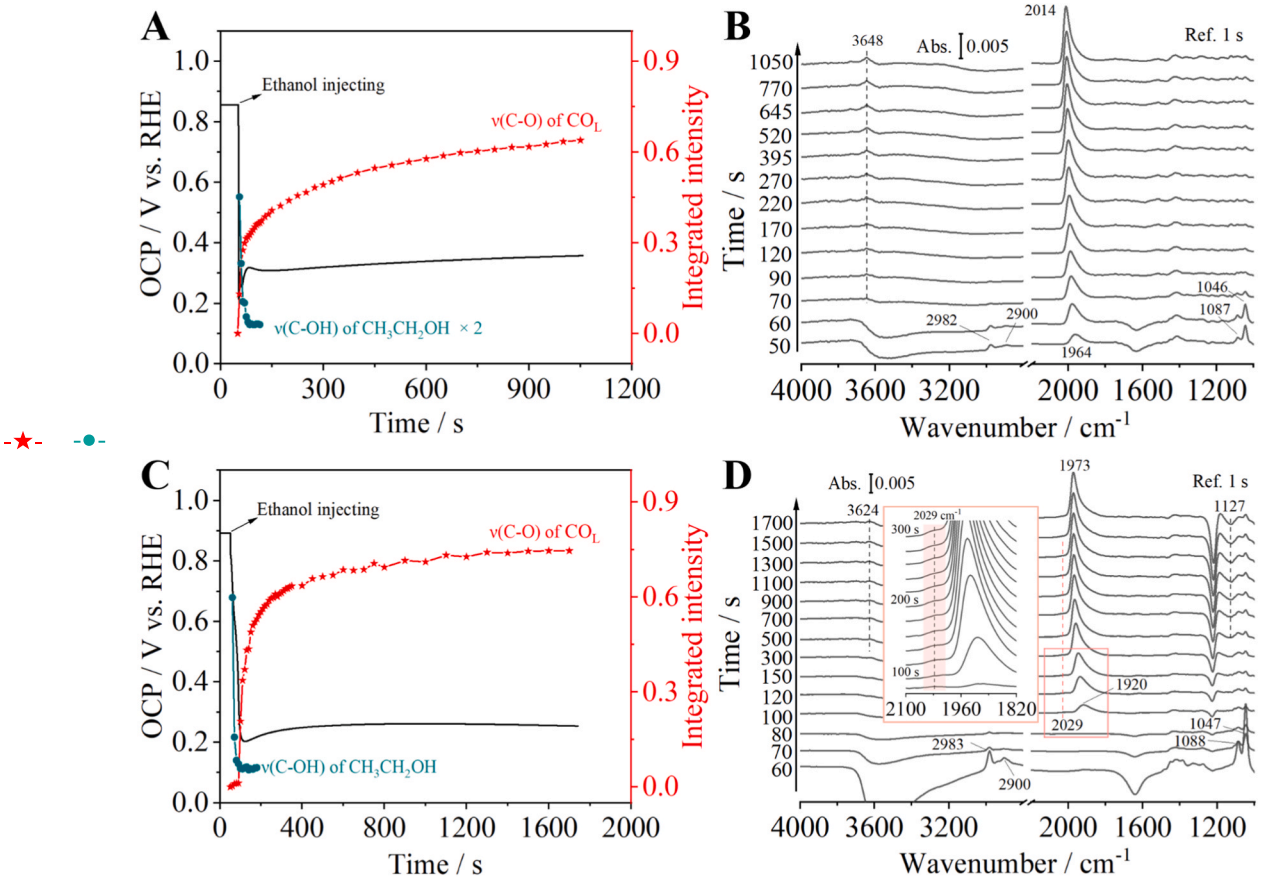

Fig. 1. (A) and (C) show time-dependent OCP variation curves (OCP-t) after 1 M ethanol dosing to Ir surface in 0.1 M $HClO_4$ and 0.1 M NaOH; (B) and (D) show the corresponding real-time ATR-SEIRA spectra collected on Ir electrode, taken single-beam spectrum in neat electrolyte as the reference spectrum with the spectral resolution of 8 cm^{-1}. and profile in (A) and (C) is the time-dependent intensity variation of $\nu(CO_L)$ and ν(C-OH) of CH_3CH_2OH taken from (B) and (D), respectively. The inset in (D) is the enlarged image from 1820 to 2100 cm^{-1}.

ethanol. Correspondingly, real-time ATR-SEIRA spectra (Fig. 1B and D) clearly show the feature bands of interfacial ethanol and/or ethoxy (2900 and 2983 cm^{-1} for the C-H stretching vibration, ν(C-H); 1046 and 1088 cm^{-1} for the O-H stretching vibration, ν(C-OH)) [9], and linearly-adsorbed CO_{ad} species (C-O stretching model vibration of CO_L ($\nu(CO_L)$) at 1964–2013 and 1912–1973 cm^{-1} in acidic and alkaline media, respectively) [42,51]. The interfacial ethanol/ethoxy species disappeared and CO_L emerged within 100 s after ethanol injection, suggesting that interfacial ethanol can readily undergo self-dissociation via splitting C-C bond and synchronous dehydrogenation in alkaline and acidic electrolytes. Meanwhile, the saturate integrated intensity of $\nu(CO_L)$ was higher in alkaline media than that in acidic media, which may be highly related to the increasing electro-negativity of Ir electrode in the local double-layer environment with abundant OH^- [7,42]. Interestingly, ethanol self-dissociation on Pt and Ir surface can take place both in alkaline and acidic electrolytes [52], whereas on Pd and Rh surfaces it only happens in alkaline media rather than acidic media [7, 9]. This difference of ethanol self-dissociation on Pt-group metal surfaces is an interesting and open topic to further study.

3.1.2. Surface-bonded H species at Ir sites

It should be noted that a very weak band at 2029 cm^{-1} synchronously appeared with the CO_L species in alkaline media (Fig. 1D). Considering the corresponding OCP was at 0.25 V in the hydrogen adsorption potential region in alkaline media, this weak band is envisioned for the Ir-H_{ad} species [49]. To confirm the existence of Ir-H_{ad} species, in situ electrochemical ATR-SEIRA spectra were collected during the potential negative scanning from 0.5 to − 0.3 V in Ar-saturated 0.1 M $HClO_4$ and 0.1 M NaOH solution. As shown in Fig. 2, the band centered at ca. 2086 and 2045 cm^{-1} was detected from ca. 0.05 V in 0.1 M $HClO_4$ and 0.25 V in 0.1 M NaOH solution, being assigned to the Ir-H_{ad} species, respectively [53,54]. This potential difference in acidic and alkaline media can also explain why we only detected the Ir-H_{ad} species in 0.1 M NaOH + 1 M CH_3CH_2OH solution rather than 0.1 M $HClO_4$ + 1 M CH_3CH_2OH, as shown in Figs. 1B and 1D. Specifically, the spectral results in Fig. 2 can sufficiently suggest that H_{ad} species inhabited stably at Ir sites as the potentials were lower than 0.05 and 0.25 V in acidic and alkaline media, respectively. Considering the stable OCP at the Ir electrode in 0.1 M $HClO_4$ + 1 M CH_3CH_2OH was at ca. 0.25 V, thus it should be reasonable that Ir-H_{ad} species cannot be detected under this condition. Meanwhile, this result also indirectly demonstrates the pH-dependent surface behavior on the electrode [53, 54].

In addition, another important point for Ir-H_{ad} species is whether they originate from ethanol dehydrogenation or water splitting on the Ir surface. To understand it, ethanol was introduced onto the Ir electrode when the electrode potential was controlled at 0.3 V in Ar-saturated 0.1 M NaOH, where the water-splitting should be negligible (see the cyclic voltammograms in Fig. 4 below). As shown in Fig. 3A, the surface ethanol/ethoxy species were quickly consumed on the Ir surface, since the bands at 2981, 2903, 1087, and 1046 cm^{-1} disappeared within 20 s. Alternatively, the band at 1914–1952 cm^{-1} (CO_{ad} species) and 2038 cm^{-1} (Ir-H_{ad} species) began to emerge synchronously. Thus, it indicates that CO_{ad} and Ir-H_{ad} species mainly come from the surface dissociation of ethanol/ethoxy species. Meanwhile, for the sake of rigor, here it's necessary to eliminate the possibility that the band at 2038 cm^{-1} was due to the CO_{ad} species. Thus, in situ ATR-SEIRA spectra were collected on Ir electrode in Ar-saturated 0.1 M NaOH as the high-purity CO gas bubbling at 0 V. As shown in Fig. 3B, a weak IR band was detected at ca. 2042 cm^{-1} before CO dosing, and with CO gas continuous introducing, the feature band of CO_{ad} species shows at the frequency range of 1993–2006 cm^{-1} and the band intensity gradually increase with the CO coverage increasing. Therefore, the ca. 2038–2042 cm^{-1} band should be assigned to the Ir-H_{ad} species.

Along this line, it can be said that the surface self-dissociation of ethanol at the Ir electrode generates the CO_{ad} and Ir-H_{ad} species, being roughly written as $CH_3CH_2OH \rightarrow CH_x + CO_{ad} + H_{ad}$ [29]. CO_{ad} species can be detected in acidic and alkaline media, whereas H_{ad} species only be observed in alkaline media, which is mainly due to the pH-dependent difference of hydrogen binding on the electrode as discussed above.

3.1.3. EOR on the Ir electrodes

The Cyclic Voltammetric (CV) profiles at Ir electrodes are shown in Fig. 4 [54,55]. Compared with other Pt-group metals, the EOR onset potential on Ir surface in alkaline media is at least 100 mV lower [7,9]. Nevertheless, the forward scanning peak current density (J_f) on Ir is much lower than that on Pd, Pt and Rh electrodes, which should be enhanced through component and structure modulation as described elsewhere [31,34,40]. The onset oxidation potential and the peak potential of EOR in acidic media is higher than that in alkaline media, which could be owning to the easier formation of OH_{ad} species in alkaline media [56]. This is also supported by the CO electrooxidation on the Ir electrode, which has been described in our previous work [42]. In short, it mainly follows the so-called Langmuir-Hinshelwood mechanism (L-H mechanism: Ir-CO_{ad} + Ir-OH_{ad} → 2Ir + CO_2 + H^+ + $2e^-$) [42, 57,58], Besides, in alkaline media, it may also follow the Eley-Rideal mechanism (E-R mechanism: CO + $2OH^-$ → CO_2 + H_2O + $2e^-$) [59, 60], especially at low potentials, which could be used to understand the lower EOR onset potential in alkaline media.

Accordingly, in situ electrochemical ATR-SEIRA spectra for EOR on Ir in 0.1 M $HClO_4$ and 0.1 M NaOH are shown in Figs. 5A and 5B, respectively. It can observe the ν(C-O) band of CO_L (at 2006–2033 cm^{-1} in acidic media; at 1961–1994 cm^{-1} in alkaline media) and co-adsorbed interfacial free water (H_2O_{free}, ν(O-H): 3600–3660 cm^{-1}). A weak band at ca. 1636 cm^{-1} can be assigned to the H-O-H bending mode of interfacial water, which also might be associated with the C═O stretching vibration of the adsorbed acetyl or acetaldehyde species [38,61]. On the other hand, in situ IRAS (Fig. 5C and D) was also used to identify the dissolved products. In an acidic solution, the bands at 1720, 1352, and 1289 cm^{-1} were assigned to C═O stretching of acetic acid and/or acetaldehyde, in-plane bending of -CH_3 of adsorbed acetate, respectively [22,62,63]. It indicates the production of acetic acid and/or acetaldehyde (if any). And the band at 2343 cm^{-1} is attributed to CO_2 [62]. Even at 1.0 V, the band at 1720 cm^{-1} is negligible, which indicates only a trace amount of C2 products generation. In alkaline media, the emergence of the bands at 1351, 1415, 1551, and 1716 cm^{-1} above 0.45 V can be attributed to the acetate [32]. The CO_2 appeared above 0.9 V after the thin-layer NaOH solution has been neutralized [7]. Before that, the (bi)carbonate should be the main C1 product as demonstrated before [32]. Nevertheless, we can't obtain the high-resolution feature band of (bi)carbonate, since it's usually closely overlapped with the band at

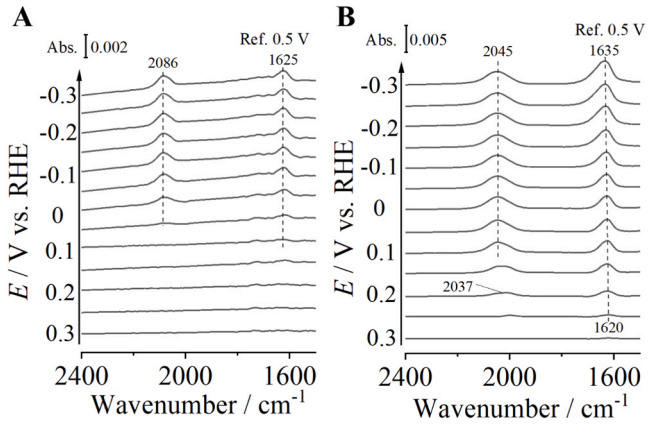

Fig. 2. In situ ATR-SEIRA spectra recorded on the Ir electrode during the potential negative scanning from 0.5 to − 0.3 V in an Ar-saturated (A) 0.1 M $HClO_4$ and (B) 0.1 M NaOH solution, taken single-beam spectrum at 0.5 V as the reference spectrum.

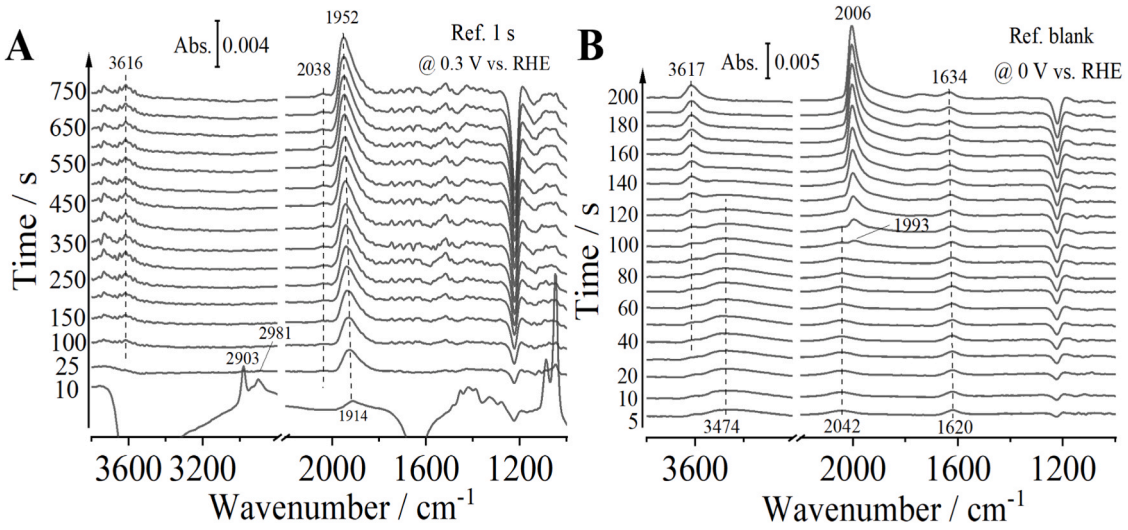

Fig. 3. (A) Real-time ATR-SEIRA spectra collected on the Ir electrode in an Ar-saturated 0.1 M NaOH with ethanol injecting at 0.3 V, taken single-beam spectrum in the neat electrolyte as the reference spectrum; (B) Real-time ATR-SEIRA spectra collected on Ir electrode at 0 V in an Ar-saturated 0.1 M NaOH, the CO bubbling started at 100 s, taken single-beam spectrum in neat electrolyte as the reference spectrum.

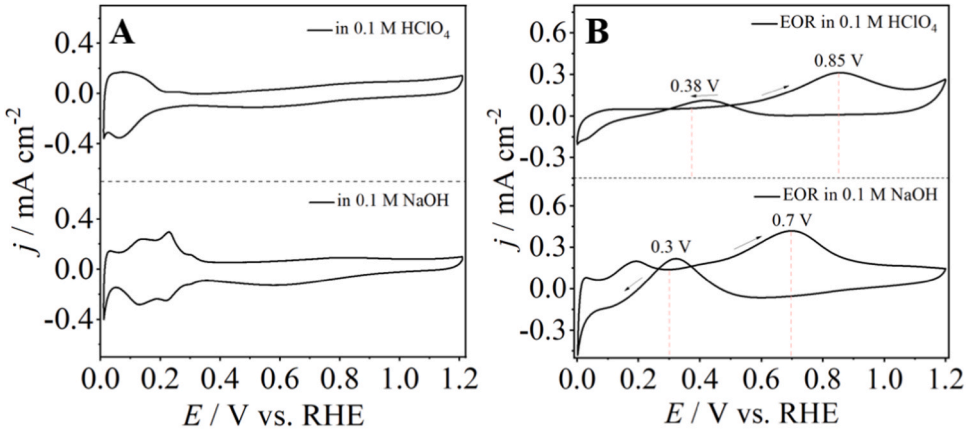

Fig. 4. CVs collected on the Ir electrode in 0.1 M $HClO_4$ or NaOH solution with or without 1 M CH_3CH_2OH at a scan rate of 10 mV s^{-1}. The current densities are normalized to the geometric surface area.

1415 cm^{-1} of acetate [16].

Thus, the potential-dependent distribution of intermediates and products can be obtained, as shown in Figs. 5E and 5F. In acidic media, the CO_{ad} band intensities started to decrease from ca. 0.35 V, being the same as the above-mentioned OH_{ad} formation potential on the Ir surface. The band of C2 products initially appeared at 0.5 V and its intensity doesn't significantly increase until 0.9 V, which suggests that ethanol-to-CO_2 oxidation might predominately contribute to the faradaic current at 0.5 ~ 0.9 V (vide infra). In alkaline media, the band intensities of CO_{ad} species started to decrease from 0.4 V. Meanwhile, the acetate was apparently generated from 0.5 V, and the acetate quickly increased from 0.5 to 0.9 V with an apparent decrease of the CO_{ad} band intensities. It indicates that EOR C1 and C2 reaction pathways co-exist and contribute to the main oxidation peak. Thus, we can conclude that EOR on Ir electrodes follow the so-called Dual-Pathway Mechanism, where CO_{ad} (and CH_x) is the main C1 intermediates that is responsible for the CO_2 (carbonate) generation, and acetic acid (acetate) is the main C2 products.

3.2. Apparent faraday efficiency of C1 pathway by QEIAS

QEIAS method based on the combination of in situ electrochemical ATR-SEIRAS, IRAS, and TIAS was used to roughly calculate the apparent FE_{C1} (also denoted as η in this section) on Ir electrode both in alkaline and acidic media. Since the anodic EOR potentials exceeding 0.8 V vs. RHE are almost inaccessible in real DEFC devices [6], thus the FE_{C1} for EOR was tested from 0.5 to 0.8 V (the main oxidation potential region). Meanwhile, considering the difference of EOR products and their dissolubility in the acidic and alkaline media, different strategies were adopted in two conditions.

First, the apparent FE_{C1} in acidic media (η_{acidic}) was quasi-quantitatively determined via the peak integration method developed by Weaver et al. [46], also described as Eq. (3) in the previous work [21, 64].

$$\eta_{acidic} = \frac{6n(CO_2)}{6n(CO_2) + 4n(CH_3COOH)} \times 100\% \quad (3)$$

where n means the quantities (mol cm^{-2}) of a given species inside the thin-layer cavity under IRAS configuration during the EOR process, and the number 6 and 4 come from the electron transferring amount during the production of one CO_2 and CH_3COOH, respectively. Meanwhile, n follows the relationship $n = \frac{A_i}{\varepsilon_i}$, where A_i is the respective integrated absorbance of the corresponding species (can be obtained from Fig. 5C) and ε_i is the value of the effective integrated molar absorptivity of

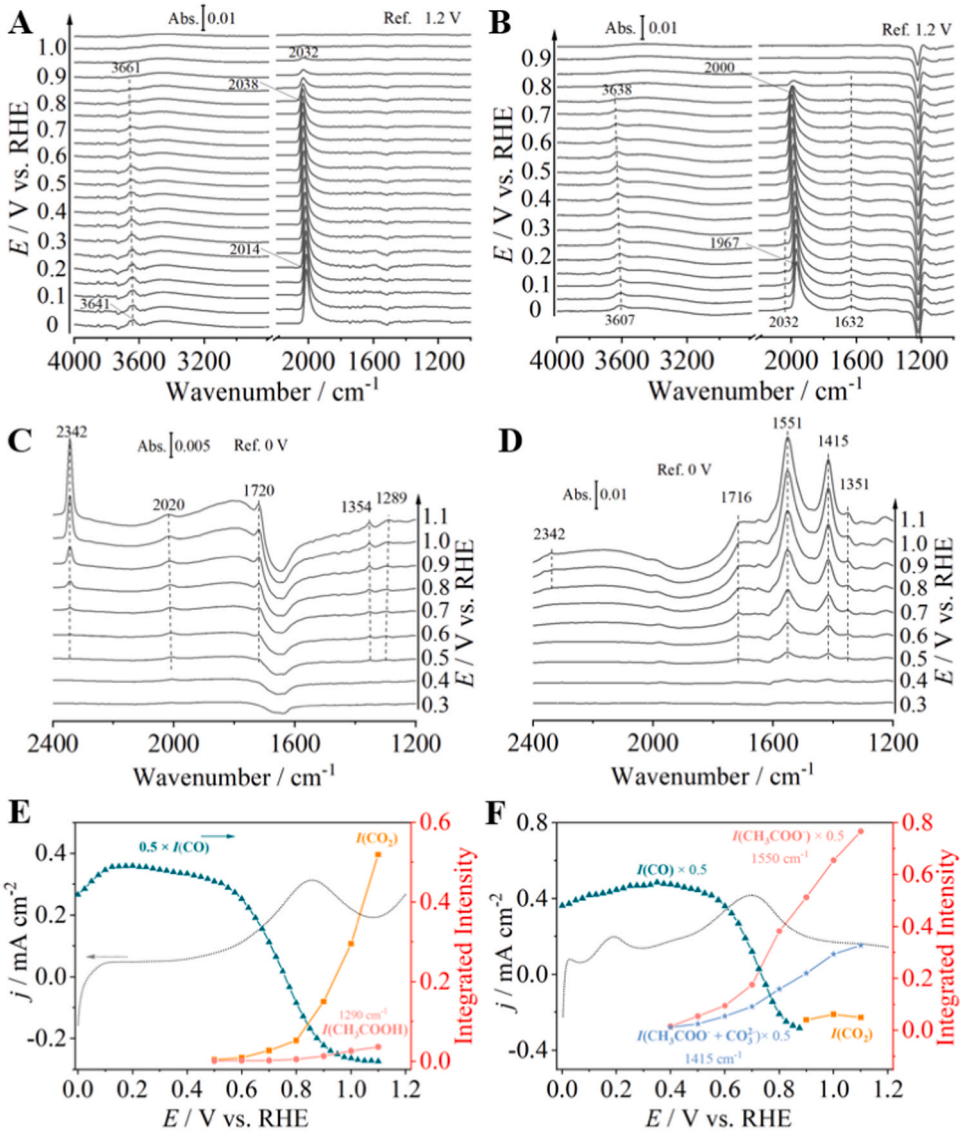

Fig. 5. Real-time ATR-SEIRA spectra collected on the Ir film electrode in (A) 0.1 M $HClO_4$ + 1 M CH_3CH_2OH and (B) 0.1 M NaOH + 1 M CH_3CH_2OH from 0 V to 1.2 V at a potential scan rate of 5 mV s^{-1}, taken the single-beam spectrum at 1.2 V as the reference spectrum. IRA spectra collected in (C) 0.1 M $HClO_4$ + 1 M CH_3CH_2OH and (D) 0.1 M NaOH + 1 M CH_3CH_2OH from 0 V to 1.2 V, taken the single-beam spectrum at 0 V as the reference spectrum. The spectral resolution is 8 cm^{-1}. (E) and (F) show the potential-dependent band intensity variation of CO_L (~2000 cm^{-1}), acetic acid (1290 cm^{-1})/acetate (1550 cm^{-1}), and CO_2 (2341 cm^{-1}) in 0.1 M $HClO_4$ + 1 M CH_3CH_2OH and 0.1 M NaOH + 1 M CH_3CH_2OH, respectively. The black dash profiles in (E) and (F) are the corresponding forward scanning CVs which are as similar as those in Fig. 4B.

species *i*. The values of ε are taken from the work by Weaver et al. [65, 66], and equal 3.5×10^4 and 5.8×10^3 M^{-1} cm^{-2} for CO_2 and CH_3COOH, respectively.

Thus, as shown in Table 1, we can obtain that the FE_{C1} was roughly calculated to be 49.9%, 55.4%, 76.4%, and 74.2% at 0.5, 0.6, 0.7 and 0.8 V at Ir electrode in acidic media (Table 1, Fig. S2A), which shows a relative error of ca. 9% in acidic media compared with that obtained from HPLC (see Section 3.3).

On the other hand, although the amount of products could be inaccurate through in-situ FTIR in alkaline media, FE_{C1} in alkaline media ($\eta_{alkaline}$) on the Ir electrode can be roughly estimated as follows:[16].

Table 1
The parameters listed for calculating the FE_{C1} of EOR in acidic media (η_{acidic}).

Potential	ε (CO_2) / M^{-1} cm^{-2}	ε (CH_3COOH) / M^{-1} cm^{-2}	A (CO_2)[a] / cm^{-1}	A (CH_3COOH)[a] / cm^{-1}	n (CO_2)[b] / mol cm^{-2}	n (CH_3COOH)[b] / mol cm^{-2}	η_{acidic}[c]
0.5 V	3.5×10^4	5.8×10^3	0.004	0.001	6.857×10^{-7}	6.896×10^{-7}	49.9%
0.6 V	3.5×10^4	5.8×10^3	0.01	0.002	1.714×10^{-6}	1.379×10^{-6}	55.4%
0.7 V	3.5×10^4	5.8×10^3	0.026	0.002	4.457×10^{-6}	1.379×10^{-6}	76.4%
0.8 V	3.5×10^4	5.8×10^3	0.058	0.005	9.943×10^{-6}	3.448×10^{-6}	74.2%

[a] It can be obtained from Fig. 5C.

[b] It can be obtained from equation $n = \frac{A_i}{\varepsilon_i}$.

[c] It can be obtained from Eq. (3).

$$\eta_{\text{alkaline}} = \frac{6Cr(CO_3^{2-})}{6Cr(CO_3^{2-}) + 4Cr(acetate)} \times 100\% \quad (4)$$

where *Cr* means the relative concentration of the corresponding species in the thin layer under the in-situ IRAS configuration at each potential, and the number 6 and 4 also come from the electron transferring amount during the production of one equivalent CO_2 and CH_3COOH, respectively.

Cr(acetate) in the thin-layer under the electrochemical reaction conditions can be estimated through an external standard method based on the Beer-Lambert Law. The intensity of the feature band of acetate at 1550 cm^{-1} in TIAS (Fig. 6B) was readily adopted to correlate a linear relationship with its concentrations, being well plotted in Fig. 6D.

Nevertheless, $Cr(CO_3^{2-})$ is relatively difficult to be calculated, since the feature band of (bi)carbonate (~1400 cm^{-1}) is usually closely overlapped by the band of acetate centered at ca. 1415 cm^{-1} [16]. In other words, the IRAS bands at ca. 1415 cm^{-1} should involve the contribution from (bi)carbonate species. Fortunately, since the distribution of various products at each potential should be fixed, their IRAS feature band intensity ratio should also be a constant that is highly correlated with the product distribution according to the Beer-Lambert Law. This essentially provides a possibility for us to establish a relationship between the concentration ratio of species with their feature band intensity ratio.

Here, the band intensity ratio (*r*, *I*(1550)/*I*(1415)) between the 1550 and 1415 cm^{-1} band is roughly denoted as the following equation according to the Beer-Lambert Law,

$$r = \frac{I(1550)}{I(1415)} = \frac{\alpha(acetate) \times Cr(acetate) \times l}{0.377\alpha(acetate) \times Cr(acetate) \times l + \alpha(CO_3^{2-}) \times Cr(CO_3^{2-}) \times l} \quad (5)$$

where α is the effective infrared absorption coefficient, l is the optical length that should be the same for one IRAS measurement, an 0.377 comes from the value of *I*(1415)/*I*(1550) for the neat acetate aqueous solution [30].

Given $s = \alpha(CO_3^{2-})/\alpha(acetate)$ and $k = Cr(CO_3^{2-})/Cr(acetate)$, from Eq. (5), we can obtain a simple linear correlation between $1/r$ and k with its slope to be s as follows,

$$1/r = 0{\cdot}377 + sk \quad (6)$$

Based on the TIA spectra of a standard solution containing 50 mM CH_3COONa and 0 ~ 20 mM Na_2CO_3 (Fig. 6C), the according linear curve between $1/r$ and k can be plotted in Fig. 6E. Thus Eq. (6) can also be written as follows,

$$1/r = 0{\cdot}377 + 1{\cdot}609k \quad (7)$$

Thereby, the concentration ratio k during EOR at each potential could be readily obtained and listed in Table 2. Furthermore, the k

Table 2
The parameters listed for calculating the FE_{C1} of EOR in alkaline media ($\eta_{alkaline}$).

Potential	r^a	s^b	k^c	$\eta_{alkaline}{}^d$
0.5 V	2.317	1.609	0.034	4.8%
0.6 V	1.882	1.609	0.096	12.6%
0.7 V	1.984	1.609	0.079	10.6%
0.8 V	2.470	1.609	0.017	2.5%

[a] The band intensity ratio between 1550 and 1415 cm^{-1} band taken from Fig. 5D.
[b] It's obtained from Fig. 6E.
[c] it can be obtained from Eq. (7).
[d] It can be obtained from Eq. (8).

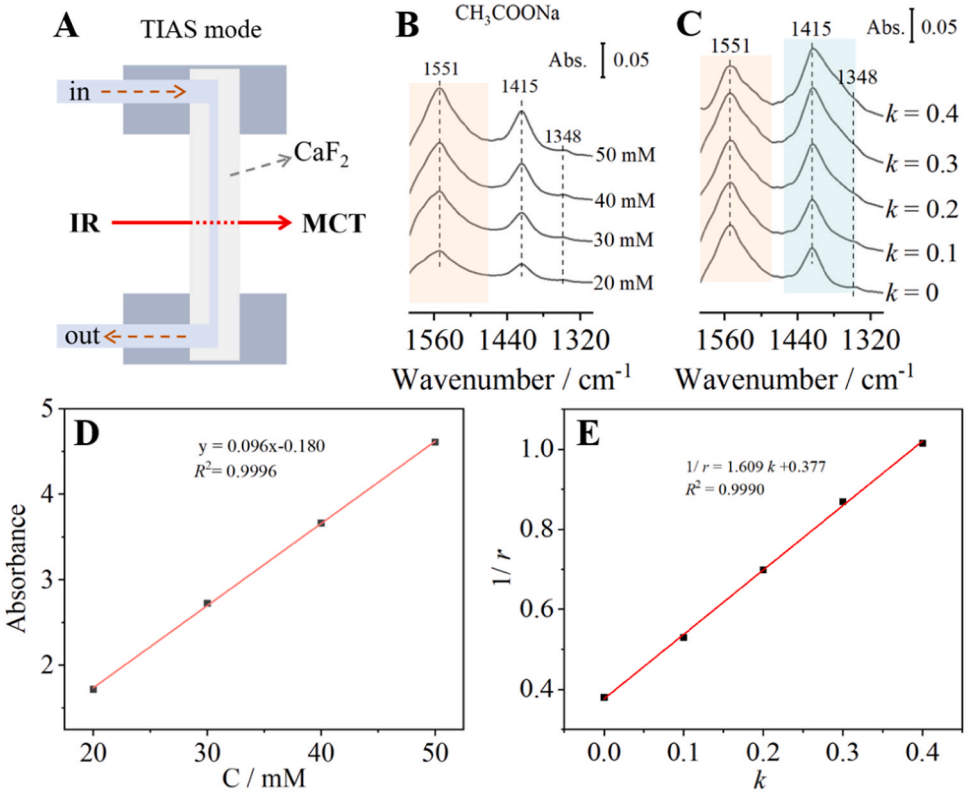

Fig. 6. (A) The schematic illustration of the flow cell of TIAS; (B) TIA spectra of 20 ~ 50 mM CH_3COONa solution and (C) 50 mM CH_3COONa solution containing 0 ~ 20 mM Na_2CO_3, taken the single-beam spectrum of ultrapure water as the reference spectrum. (D) Typical linear fitting curve of the band absorbance at 1551 cm^{-1} taken from (B) with the concentration. (E) typical linear fitting curve of the band intensity ratio (*r*) between 1550 and 1415 cm^{-1} band taken from (D) with its corresponding *k* value, which can get a *s* value of 1.609.

values at different potentials can be plugged into the following Eq. (8) which is obtained based on Eq. (4) to obtain the FE_{C1} in alkaline media (also denoted as $\eta_{alkaline}$).

$$\eta_{alkaline} = 1/(1+2/3k) \times 100\% \quad (8)$$

Thus, the FE_{C1} in alkaline media can be calculated and the values are 4.8%, 12.6%, 10.6%, and 2.5% at 0.5, 0.6, 0.7, and 0.8 V, respectively (Table 2 and Fig. S2B). The relative error is as small as 2% compared with that obtained from HPLC (see Section 3.3), which claims that the QEIAS method is feasible.

3.3. Apparent Faraday Efficiency of C1 Pathway by NMR and HPLC

As stated above, to confirm the feasibility of QEIAS method towards the estimation of FE_{C1}, here we further comparatively measured the FE_{C1} for EOR within 0.5–0.8 V according to Eqs. (1) and (2) described in experimental section [16,30,32]. First, ethanol oxidation was performed at a constant applied potential (0.5~ 0.8 V) for at least 24 h. The reaction residual was prepared as the sample to carry out the ^{1}H NMR and HPLC measurement. As shown in Fig. 7 A, the only detectable C2 product is acetate (the chemical shift at 1.8 ppm) in alkaline media and acetic acid (the chemical shift at 2.0 ppm) in acidic media during EOR on Ir. Note that acetaldehyde was not detected in either case, although acetaldehyde could be one of the important C2 intermediates of EOR, especially in acidic media [52,67]. This may suggest the amount of acetaldehyde under the detection limited of NMR. Moreover, the band at 1720 cm^{-1} is negligible even at 1.0 V in Fig. 5C, suggesting that only a trace amount of acetaldehyde and acetic acid were produced during the EOR in acidic media [23]. However, we still cannot exclude the production of trace acetaldehyde in the EOR process, meanwhile, the characteristic peak of acetaldehyde and acetic acid is overlapped in the HPLC profile (Fig. S3). Therefore, here we roughly consider acetaldehyde and acetic acid as one to calculate the Faraday efficiency, even if the error exists. The external standard curve of acetate has been

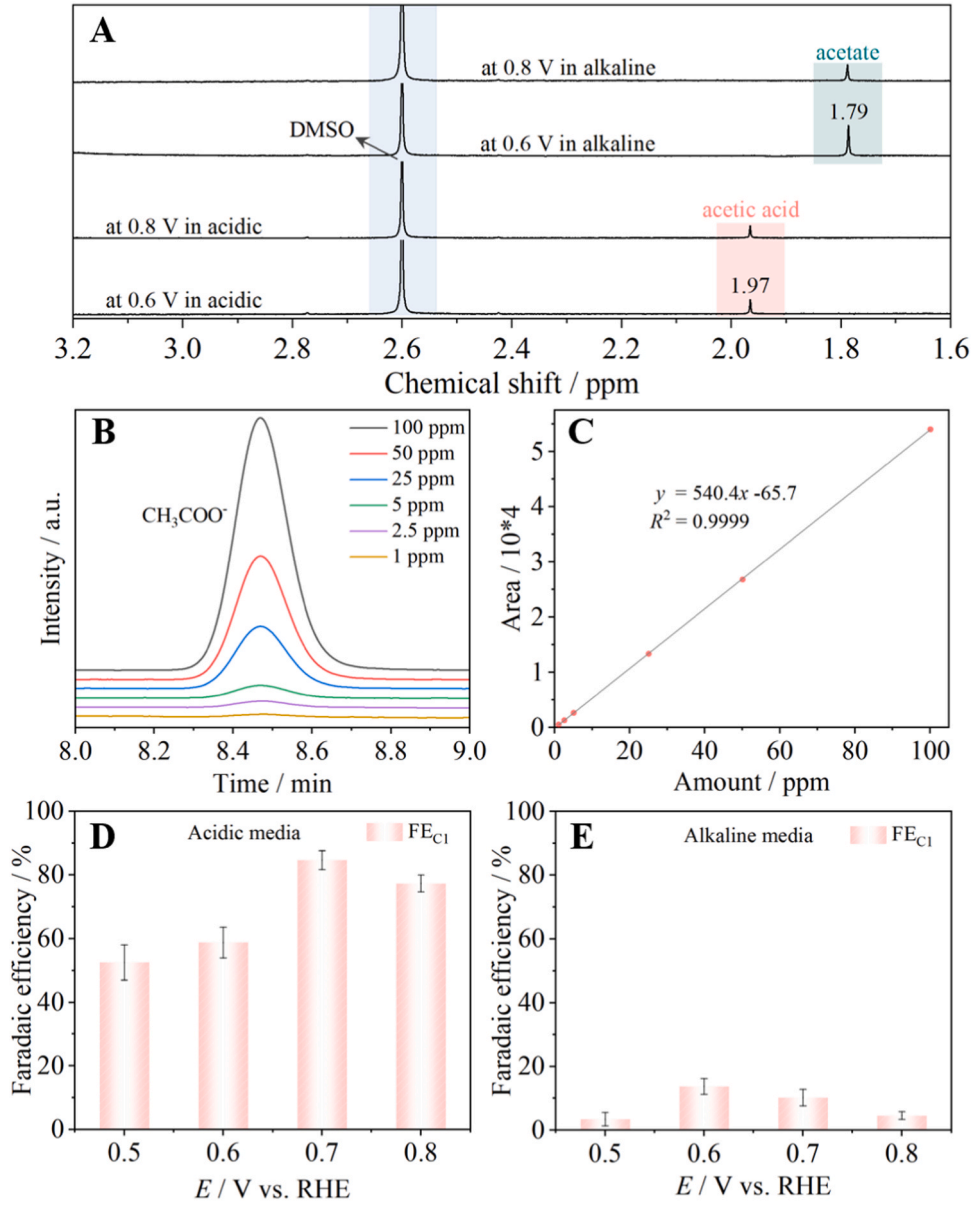

Fig. 7. (A) Typical ^{1}H NMR spectra of the residual electrolyte after a 24-hour electrolysis on the Ir surface at 0.6 and 0.8 V vs. RHE, respectively. Chemical shift (δ): Dimethyl sulphoxide ($\delta = 2.6$ ppm), acetate ($\delta = 1.79$ ppm), and acetic acid ($\delta = 1.97$ ppm). (B) Typical HPLC profiles of the standard acetate solution with various concentration, the retention time of acetate is ca. 8.47 min (C) The external standard curve of the acetate established via the HPLC results in (B). The FE_{C1} of EOR at different electrode potentials in (C) 0.1 M $HClO_4$ and (D) 0.1 M NaOH obtained based on HPLC measurements.

established as shown in Fig. 7B and 7C, therefore, the concentration of acetate in the reaction residual can be calculated by Eq. (1). And thus the FE_{C1} was calculated to be 52.5%, 58.7%, 84.6%, and 77.3% at 0.5, 0.6, 0.7 and 0.8 V over Ir electrode in acidic media (Fig. 7D), which are much higher than those in alkaline media (FE_{C1} is 3.4%, 13.7%, 10.2%, and 4.6% at 0.5, 0.6, 0.7, and 0.8 V (Fig. 7E), respectively). As stated above, the relative error is as small as 2% and 9% compared with that obtained from HPLC in alkaline and acidic media, respectively. Once again, this can suggest that our QEIAS method is feasible to reveal the selectivity of surface catalytic reactions.

Based on the above discussion of the ethanol self-dissociation and oxidation on Ir, it could be convincible that Ir catalysts might be more efficient for ethanol complete oxidation than other Pt-group metallic catalysts, especially in acidic media. Nevertheless, the EOR current density on Ir should be further enhanced, which likely needs to quickly remove the strong adsorbents such as CO_{ad} and CH_x species on Ir surface. According to our previous study on Rh, it might be effective to fabricate oxyphilic metallic or nonmetallic atoms (or clusters) around Ir nano-domains to form a bifunctional effect interface as directed by the Langmuir-Hinshelwood mechanism, which should be further carried out in near future.

4. Conclusions

In summary, the ethanol dissociation and oxidation evolution behavior on Ir film have been studied. The in-situ ATR-SEIRA spectral results show that surface self-dissociation of ethanol at the Ir electrode can generate the C1 intermediates (CO_{ad} and CH_x species) and Ir-H_{ad} species. Meanwhile, CVs show that the EOR onset potential on the Ir surface in alkaline media is at least 100 mV lower than that in acidic media, and the current density on Ir is much lower than that on Pd, Pt, and Rh electrodes. Further, the in situ electrochemical ATR-SEIRA and IRA spectral results during EOR on Ir electrode indicated that EOR still followed the so-called dual-pathway mechanism, and CO_2 (or carbonate) and acetic acid (or acetate) is the C1 and C2 products, respectively. On the basis of this understanding, a QEIAS analysis method consisting of ATR-SEIRAS, IRAS, and TIAS was developed to estimate the apparent Faradaic efficiency of EOR C1 pathway, and it is ca. 2.5–12.6% and 49.9–84.6% at 0.5–0.8 V in alkaline and acidic media, respectively. Moreover, the FE_{C1} results were confirmed by the external standard method based on the measurements of ^{1}H NMR and HPLC to the reaction residual. The results show that the relative errors of FE_{C1} between two methods are 2–9% both in alkaline and acidic media. Thus, it could be convincible that Ir catalysts might be more efficient for ethanol complete oxidation than other Pt-group mono-metallic catalysts, especially in acidic media. Meanwhile, it's still critical to rationally design new Ir-based catalysts to obtain high activity, long-term stability and high C1-pathway selectivity.

CRediT authorship contribution statement

Rui-Lin Wei: Investigation, Writing – original draft. **Yue Liu:** Investigation, Writing – review & editing. **Yao-Yue Yang:** Conceptualization, Writing – review & editing, Funding acquisition.

Declaration of Competing Interest

The authors declare that they have no known competing financial interests or personal relationships that could have appeared to influence the work reported in this paper.

Data Availability

Data will be made available on request.

Acknowledgements

This work was supported by the National Natural Science Foundation of China (No. 22172121), the Natural Science Foundation of Sichuan Province (No. 2023NSFSC1076), the Young Talent Project of National Ethic Affairs Commission, and the Fundamental Research Funds for the Central Universities (No. ZYN2024002), Southwest Minzu University.

Appendix A. Supporting information

Supplementary data associated with this article can be found in the online version at doi:10.1016/j.apcatb.2023.123638.

References

[1] J. Rogelj, O. Geden, A. Cowie, A. Reisinger, Three ways to improve net-zero emissions targets: three ways to fix, Nature 591 (2021) 365–368, https://doi.org/10.1038/d41586-021-00662-3.
[2] S. Davis, N. Lewis, M. Shaner, S. Aggarwal, D. Arent, I. Azevedo, S. Benson, T. Bradley, J. Brouwer, Y. Chiang, C. Clack, A. Cohen, S. Doig, J. Edmonds, P. Fennell, C. Field, B. Hannegan, B. Hodge, M. Hoffert, E. Ingersoll, P. Jaramillo, K. Lackner, K. Mach, M. Mastrandrea, J. Ogden, P. Peterson, D. Sanchez, D. Sperling, J. Stagner, J. Trancik, C.J. Yang, K. Caldeira, Net-zero emissions energy systems, Science 360 (2018), eaas9793, https://doi.org/10.1126/science.aas9793.
[3] S. Badwal, S. Giddey, A. Kulkarni, J. Goel, S. Basu, Direct ethanol fuel cells for transport and stationary applications - a comprehensive review, Appl. Energ. 145 (2015) 80–103, https://doi.org/10.1016/j.apenergy.2015.02.002.
[4] C. Bianchini, P. Shen, Palladium-based electrocatalysts for alcohol oxidation in half cells and in direct alcohol fuel cells, Chem. Rev. 109 (2009) 4183–4206, https://doi.org/10.1021/cr9000995.
[5] J. Chang, G. Wang, M. Wang, Q. Wang, B. Li, H. Zhou, Y. Zhu, W. Zhang, M. Omer, N. Orlovskaya, Q. Ma, M. Gu, Z. Feng, G. Wang, Y. Yang, Improving Pd-N-C fuel cell electrocatalysts through fluorination-driven rearrangements of local coordination environment, Nat. Energy 6 (2021) 1144–1153, https://doi.org/10.1038/s41560-021-00940-4.
[6] J. Chang, G. Wang, X. Chang, Z. Yang, H. Wang, B. Li, W. Zhang, L. Kovarik, Y. Du, N. Orlovskaya, B. Xu, G. Wang, Y. Yang, Interface synergism and engineering of Pd/Co@N-C for direct ethanol fuel cells, Nat. Commun. 14 (2023), 1346, https://doi.org/10.1038/s41467-023-37011-z.
[7] C. Zhu, B. Lan, R. Wei, C. Wang, Y. Yang, Potential-dependent selectivity of ethanol complete oxidation on Rh electrode in alkaline media: a synergistic study of electrochemical ATR-SEIRAS and IRAS, ACS Catal. 9 (2019) 4046–4053, https://doi.org/10.1021/acscatal.9b00138.
[8] T. Sheng, Y. Xu, Y. Jiang, L. Huang, N. Tian, Z. Zhou, I. Broadwell, S. Sun, Structure design and performance tuning of nanomaterials for electrochemical energy conversion and storage, Acc. Chem. Res. 49 (2016) 2569–2577, https://doi.org/10.1021/acs.accounts.6b00485.
[9] Y. Yang, J. Ren, Q. Li, Z. Zhou, S. Sun, W. Cai, Electrocatalysis of ethanol on a Pd electrode in alkaline media: an in situ attenuated total reflection surface-enhanced infrared absorption spectroscopy study, ACS Catal. 4 (2014) 798–803, https://doi.org/10.1021/cs401198t.
[10] R. Kavanagh, X. Cao, W. Lin, C. Hardacre, P. Hu, Origin of low CO_2 selectivity on platinum in the direct ethanol fuel cell, Angew. Chem. Int. Ed. 51 (2012) 1572–1575, https://doi.org/10.1002/anie.201104990.
[11] J. Sulaiman, S. Zhu, Z. Xiang, Q. Chang, M. Shao, Pt-Ni octahedra as electrocatalysts for the ethanol electro-oxidation reaction, ACS Catal. 7 (2017) 5134–5141, https://doi.org/10.1021/acscatal.7b01435.
[12] K. Jiang, P. Wang, S. Guo, X. Zhang, X. Shen, G. Lu, D. Su, X. Huang, Ordered PdCu-based nanoparticles as bifunctional oxygen-reduction and ethanol-oxidation electrocatalysts, Angew. Chem. Int. Ed. 55 (2016) 9030–9035, https://doi.org/10.1002/ange.201603022.
[13] D. Wu, K. Kusada, T. Yamamoto, T. Toriyama, S. Matsumura, S. Kawaguchi, Y. Kubota, H. Kitagawa, Platinum-group-metal high-entropy-alloy nanoparticles, J. Am. Chem. Soc. 142 (2020) 13833–13838, https://doi.org/10.1021/jacs.0c04807.
[14] R. Rizo, G. García, Electrocatalysis in direct ethanol fuel cells, in: A.J. Bard (Ed.), Encyclopedia of Electrochemistry, Wiley-VCH Verlag GmbH & Co., 2021.
[15] Y. Wang, S. Zou, W. Cai, Recent advances on electro-oxidation of ethanol on Pt- and Pd-based catalysts: from reaction mechanisms to catalytic materials, Catalysts 5 (2015) 1507–1534, https://doi.org/10.3390/catal5031507.
[16] Z. Zhou, Q. Wang, J. Lin, N. Tian, S. Sun, In situ FTIR spectroscopic studies of electrooxidation of ethanol on Pd electrode in alkaline media, Electrochim. Acta 55 (2010) 7995–7999, https://doi.org/10.1016/j.electacta.2010.02.071.
[17] W. Huang, X. Ma, H. Wang, R. Feng, J. Zhou, P. Duchesne, P. Zhang, F. Chen, N. Han, F. Zhao, J. Zhou, W. Cai, Y. Li, Promoting effect of $Ni(OH)_2$ on palladium nanocrystals leads to greatly improved operation durability for electrocatalytic ethanol oxidation in alkaline solution, Adv. Mater. 29 (2017), 1703057, https://doi.org/10.1002/adma.201703057.
[18] Z. Wu, C. Zhong, Pd-based electrocatalysts for oxygen reduction and ethanol oxidation reactions: some recent insights into structures and mechanisms,

J. Electrochem 27 (2021) 144–156, https://doi.org/10.13208/j.electrochem.201241.
[19] N.S. Nia, O. Guillén-Villafuerte, C. Griesser, G. Manning, J. Kunze-Liebhäuser, C. Arévalo, E. Pastor, G. García, W_2C-supported PtAuSn-a catalyst with the earliest ethanol oxidation onset potential and the highest ethanol conversion efficiency to CO_2 known till date, ACS Catal. 10 (2020) 1113–1122, https://doi.org/10.1021/acscatal.9b04348.
[20] K. Kim, G. Hobold, K. Steinberg, B. Gallant, Confinement effects of hollow structured Pt-Rh electrocatalysts toward complete ethanol electrooxidation, ACS Nano 17 (2023) 14176–14188, https://doi.org/10.1021/acsnano.3c05334.
[21] M. Li, D. Cullen, K. Sasaki, N. Marinkovic, K. More, R. Adzic, Ternary electrocatalysts for oxidizing ethanol to carbon dioxide: making Ir capable of splitting C-C bond, J. Am. Chem. Soc. 135 (2013) 132–141, https://doi.org/10.1021/ja306384x.
[22] A. Kowal, M. Li, M. Shao, K. Sasaki, M. Vukmirovic, J. Zhang, N. Marinkovic, P. Liu, A. Frenkel, R. Adzic, Ternary Pt/Rh/SnO_2 electrocatalysts for oxidizing ethanol to CO_2, Nat. Mater. 8 (2009) 325–330, https://doi.org/10.1038/nmat2359.
[23] Q. Chang, Y. Hong, H. Lee, J.H. Lee, D. Ologunagba, Z. Liang, J. Kim, M. Kim, J. Hong, L. Song, S. Kattel, Z. Chen, J. Chen, S. Choi, Achieving complete electrooxidation of ethanol by single atomic Rh decoration of Pt nanocubes, P. Natl. Acad. Sci. U. S. A 119 (2022), e2112109119, https://doi.org/10.1073/pnas.2112109119.
[24] R. Wu, L. Wang, A density functional theory study on the mechanism of complete ethanol oxidation on Ir(100): surface diffusion-controlled C-C bond cleavage, J. Phys. Chem. C. 124 (2020) 26953–26964, https://doi.org/10.1021/acs.jpcc.0c09495.
[25] R. Wu, K. Wiegand, L. Wang, Impact of the degree of dehydrogenation in ethanol C-C bond cleavage on Ir(100), J. Chem. Phys. 154 (2021), 054705, https://doi.org/10.1063/5.0039642.
[26] Q. He, S. Mukerjee, B. Shyam, D. Ramaker, S. Parres-Esclapez, M.J. Illan-Gomez, A. Bueno-Lopez, Promoting effect of CeO_2 in the electrocatalytic activity of rhodium for ethanol electro-oxidation, J. Power Sources 193 (2009) 408–415, https://doi.org/10.1016/j.jpowsour.2009.03.056.
[27] J. Zhang, J. Ye, Q. Fan, Y. Jiang, Y. Zhu, H. Li, Z. Cao, Q. Kuang, J. Cheng, J. Zheng, Z. Xie, Cyclic penta-twinned rhodium nanobranches as superior catalysts for ethanol electro-oxidation, J. Am. Chem. Soc. 140 (2018) 11232–11240, https://doi.org/10.1021/jacs.8b03080.
[28] H. Li, J. Ye, X. Li, J. Zhang, Y. Zhu, Z. Zhou, Y. Xue, Y. Jiang, Z. Xie, L. Zheng, Excavated RhNi alloy nanobranches enable superior CO-tolerance and CO_2 selectivity at low potentials toward ethanol electro-oxidation, J. Mater. Chem. A 7 (2019) 26266–26271, https://doi.org/10.1039/C9TA10327A.
[29] G. Yang, L. Farsi, Y. Mei, X. Xu, A. Li, N. Deskins, X. Teng, Conversion of ethanol via C-C splitting on noble metal surfaces in room-temperature liquid-phase, J. Am. Chem. Soc. 141 (2019) 9444–9447, https://doi.org/10.1021/jacs.8b13115.
[30] B. Lan, M. Huang, R. Wei, C. Wang, Q. Wang, Y. Yang, Ethanol electrooxidation on rhodium-lead catalysts in alkaline media: high mass activity, long-term durability, and considerable CO_2 selectivity, Small 16 (2020), 2004380, https://doi.org/10.1002/smll.202004380.
[31] B. Lan, Q. Wang, Z. Ma, Y. Wu, X. Jiang, W. Jia, C. Zhou, Y. Yang, Efficient electrochemical ethanol-to-CO_2 conversion at rhodium and bismuth hydroxide interfaces, Appl. Catal. B: Environ. 300 (2022), 120728, https://doi.org/10.1016/j.apcatb.2021.120728.
[32] Z. Liang, L. Song, S. Deng, Y. Zhu, E. Stavitski, R. Adzic, J. Chen, J. Wang, Direct 12-electron oxidation of ethanol on a ternary Au(core)-PtIr(shell) electrocatalyst, J. Am. Chem. Soc. 141 (2019) 9629–9636, https://doi.org/10.1021/jacs.9b03474.
[33] Q. Chang, S. Kattel, X. Li, Z. Liang, B. Tackett, S. Denny, P. Zhang, D. Su, J. Chen, Z. Chen, Enhancing C-C bond scission for efficient ethanol oxidation using PtIr nanocube electrocatalysts, ACS Catal. 9 (2019) 7618–7625, https://doi.org/10.1021/acscatal.9b02039.
[34] G. Zhang, Z. Zhang, Ir_3Pb alloy nanodendrites with high performance for ethanol electrooxidation and their enhanced durability by alloying trace Au, Inorg. Chem. Front. 7 (2020) 2231–2240, https://doi.org/10.1039/D0QI00233J.
[35] C. Prossl, M. Kubler, M. Nowroozi, S. Paul, O. Clemens, U. Kramm, Investigation of the thermal removal steps of capping agents in the synthesis of bimetallic iridium-based catalysts for the ethanol oxidation reaction, Phys. Chem. Chem. Phys. 23 (2021) 563–573, https://doi.org/10.1039/D0CP04900J.
[36] Z. Yu, R. Huang, J. Liu, G. Li, Q. Song, S. Sun, Preparation of PdCoIr tetrahedron nanocatalysts and its performance toward ethanol oxidation reaction, J. Electrochem 27 (2021) 63–75, https://doi.org/10.13208/j.electrochem.200515.
[37] W. Du, Q. Wang, D. Saxner, N. Deskins, D. Su, J. Krzanowski, A. Frenkel, X. Teng, Highly active iridium/iridium-tin/tin oxide heterogeneous nanoparticles as alternative electrocatalysts for the ethanol oxidation reaction, J. Am. Chem. Soc. 133 (2011) 15172–15183, https://doi.org/10.1021/ja205649z.
[38] W. Du, N. Deskins, D. Su, X. Teng, Iridium-ruthenium alloyed nanoparticles for the ethanol oxidation fuel cell reactions, ACS Catal. 2 (2012) 1226–1231, https://doi.org/10.1021/cs3002308.
[39] R. Wei, Y. Liu, H. Ma, X. Ma, Y. Yang, Effective ethanol-to-CO_2 electrocatalysis at iridium-bismuth oxide featuring the impressive negative shifting of the working potential, J. Energy Chem. 86 (2023) 23–31, https://doi.org/10.1016/j.jechem.2023.07.013.
[40] S. Bai, Y. Xu, K. Cao, X. Huang, Selective ethanol oxidation reaction at the Rh-SnO_2 interface, Adv. Mater. 33 (2021), 2005767, https://doi.org/10.1002/adma.202005767.
[41] M. Osawa, Dynamic processes in electrochemical reactions studied by surface-enhanced infrared absorption spectroscopy (SEIRAS), Bull. Chem. Soc. Jpn. 70 (1997) 2861–2880, https://doi.org/10.1246/bcsj.70.2861.
[42] R. Wei, M. Miao, Y. Liu, X. Jiang, Y. Yang, Electrochemical attenuated total reflection surface-enhanced infrared absorption spectroscopy insights into CO adsorption and oxidation on iridium surface, J. Phys. Chem. C. 125 (2021) 12086–12093, https://doi.org/10.1021/acs.jpcc.1c00519.
[43] Y. Yang, H. Zhang, W. Cai, Recent experimental progresses on electrochemical ATR-SEIRAS, J. Electrochem. 19 (2013) 6–16. ⟨https://jelectrochem.xmu.edu.cn/journal/vol19/iss1/1⟩.
[44] J. Li, Z. Zhou, I. Broadwell, S. Sun, In-situ infrared spectroscopic studies of electrochemical energy conversion and storage, Acc. Chem. Res. 45 (2012) 485–494, https://doi.org/10.1021/ar200215t.
[45] H. Wang, Y. Zhou, W. Cai, Recent applications of in situ ATR-IR spectroscopy in interfacial electrochemistry, Curr. Opin. Electrochem. 1 (2017) 73–79, https://doi.org/10.1016/j.coelec.2017.01.008.
[46] L. Leung, S. Chang, M. Weaver, Real-time FTIR spectroscopy as an electrochemical mechanistic probe-electrooxidation of ethanol and related species on well-defined Pt(111) surfaces, J. Electroanal. Chem. 266 (1989) 317–336, https://doi.org/10.1016/0022-0728(89)85078-8.
[47] Y. Yan, Q. Li, S. Huo, M. Ma, W. Cai, M. Osawa, Ubiquitous strategy for probing ATR surface-enhanced infrared absorption at platinum group metal−electrolyte interfaces, J. Phys. Chem. B 109 (2005) 7900–7906, https://doi.org/10.1021/jp044085s.
[48] A. Petrossians, J. Whalen, J. Weiland, F. Mansfeld, Electrodeposition and characterization of thin-film platinum-iridium alloys for biological interfaces, J. Electrochem. Soc. 158 (2011), https://doi.org/10.1149/1.3559477.
[49] R. Wei, Y. Liu, Z. Chen, W. Jia, Y. Yang, W. Cai, Ammonia oxidation on iridium electrode in alkaline media: an in situ ATR-SEIRAS study, J. Electroanal. Chem. 896 (2021), 115254, https://doi.org/10.1016/j.jelechem.2021.115254.
[50] Y. Yang, J. Ren, H. Zhang, Z. Zhou, S. Sun, W. Cai, Infrared spectroelectrochemical study of dissociation and oxidation of methanol at a palladium electrode in alkaline solution, Langmuir 29 (2013) 1709–1716, https://doi.org/10.1021/la305141q.
[51] Y. Yan, Y. Yang, B. Peng, S. Malkhandi, A. Bund, U. Stimming, W. Cai, Study of CO oxidation on polycrystalline Pt electrodes in acidic solution by ATR-SEIRAS, J. Phys. Chem. C 115 (2011) 16378–16388, https://doi.org/10.1021/jp104181y.
[52] M. Shao, R. Adzic, Electrooxidation of ethanol on a Pt electrode in acid solutions: in situ ATR-SEIRAS study, Electrochim. Acta 50 (2005) 2415–2422, https://doi.org/10.1016/j.electacta.2004.10.063.
[53] S. Zhu, X. Qin, Y. Yao, M. Shao, pH-dependent hydrogen and water binding energies on platinum surfaces as directly probed through surface-enhanced infrared absorption spectroscopy, J. Am. Chem. Soc. 142 (2020) 8748–8754, https://doi.org/10.1021/jacs.0c01104.
[54] S. Zhu, M. Shao, Electrolyte pH-dependent hydrogen binding energies and coverages on platinum, iridium, rhodium, and ruthenium surfaces, Catal. Sci. Technol. 12 (2022) 3228–3233, https://doi.org/10.1039/D2CY00385F.
[55] B. Jiang, Y. Guo, J. Kim, A. Whitten, K. Wood, K. Kani, A. Rowan, J. Henzie, Y. Yamauchi, Mesoporous metallic iridium nanosheets, J. Am. Chem. Soc. 140 (2018) 12434–12441, https://doi.org/10.1021/jacs.8b05206.
[56] L. Jiang, A. Hsu, D. Chu, R. Chen, Ethanol electro-oxidation on Pt/C and PtSn/C catalysts in alkaline and acid solutions, Int. J. Hydrog. Energy 35 (2010) 365–372, https://doi.org/10.1016/j.ijhydene.2009.10.058.
[57] N. Lebedeva, M. Koper, J. Feliu, R. van Santen, Role of crystalline defects in electrocatalysis: mechanism and kinetics of CO adlayer oxidation on stepped platinum electrodes, J. Phys. Chem. B 106 (2002) 12938–12947, https://doi.org/10.1021/jp0204105.
[58] N. Lebedeva, M. Koper, J. Feliu, R. van Santen, Mechanism and kinetics of the electrochemical CO adlayer oxidation on Pt(111), J. Electroanal. Chem. 524-525 (2002) 242–251, https://doi.org/10.1016/S0022-0728(02)00669-1.
[59] S. Sun, A. Chen, In situ FTIRS features during oxygen adsorption and carbon monoxide oxidation at a platinum electrode in dilute alkaline solutions, J. Electroanal. Chem. 323 (1992) 319–328, https://doi.org/10.1016/0022-0728(92)80019-Z.
[60] J. Spendelow, G. Lu, P. Kenis, A. Wieckowski, Electrooxidation of adsorbed CO on Pt(111) and Pt(111)/Ru in alkaline media and comparison with results from acidic media, J. Electroanal. Chem. 568 (2004) 215–224, https://doi.org/10.1016/j.jelechem.2004.01.018.
[61] X. Ma, C. Ding, H. Li, K. Jiang, S. Duan, W. Cai, Revisiting the acetaldehyde oxidation reaction on a Pt electrode by high-sensitivity and wide-frequency infrared spectroscopy, J. Phys. Chem. Lett. 11 (2020) 8727–8734, https://doi.org/10.1021/acs.jpclett.0c02558.
[62] Z. Zhou, Z. Huang, D. Chen, Q. Wang, N. Tian, S. Sun, High-index faceted platinum nanocrystals supported on carbon black as highly efficient catalysts for ethanol electrooxidation, Angew. Chem. Int. Ed. 49 (2010) 411–414, https://doi.org/10.1002/ange.200905413.
[63] F. Zhu, K. Tu, L. Huang, X. Qu, J. Zhang, H. Liao, Z. Zhou, Y. Jiang, S. Sun, High selectivity PtRh/RGO catalysts for ethanol electro-oxidation at low potentials: enhancing the efficiency of CO_2 from alcoholic groups, Electrochim. Acta 292 (2018) 208–216, https://doi.org/10.1016/j.electacta.2018.08.142.
[64] Y. Fang, D. Cao, Y. Shi, S. Guo, Q. Wang, G. Zhang, P. Cui, S. Cheng, Highly porous Pt_2Ir alloy nanocrystals as a superior catalyst with high-efficiency C-C bond cleavage for ethanol electrooxidation, J. Phys. Chem. Lett. 12 (2021) 6773–6780, https://doi.org/10.1021/acs.jpclett.1c01796.
[65] L. Leung, S. Chang, M. Weaver, Real-time FTIR spectroscopy as an electrochemical mechanistic probe: electrooxidation of ethanol and related species on well-defined

Pt (111) surfaces, J. Electroanal. Chem. Interfacial Electrochem. 266 (1989) 317–336, https://doi.org/10.1016/0022-0728(89)85078-8.
[66] P. Gao, S. Chang, Z. Zhou, M. Weaver, Electrooxidation pathways of simple alcohols at platinum in pure nonaqueous and concentrated aqueous environments as studied by real-time FTIR spectroscopy, J. Electroanal. Chem. Interfacial Electrochem. 272 (1989) 161–178, https://doi.org/10.1016/0022-0728(89)87077-9.
[67] M. Heinen, Z. Jusys, R. Behm, Ethanol, acetaldehyde and acetic acid adsorption/electrooxidation on a Pt thin film electrode under continuous electrolyte flow: an in situ ATR-FTIRS flow cell study, J. Phys. Chem. C 114 (2010) 9850–9864, https://doi.org/10.1021/jp101441q.